SunQM-3s9: Using {N,n} QM to explain the sunspot drift, the continental drift, and Sun's and Earth's magnetic dynamo

by Yi Cao
Ph.D. in biophysics
e-mail: yicaojob@yahoo.com

Abstract

In this paper, a Y*lm* cycle model with two phases has been proposed. In phase-1 of Y*lm* cycle, nLL effect induces a |nLL> mode mass peaking and upwelling below the surface of an {N,n}o orbit shell, and generates a equatorial fast flow stream at the surface. As phase-1 progress, the equatorial fast flow stream gets narrower and shallower, and eventually diminished. In phase-2 of Y*lm* cycle, |n,L,m=0..L-1> modes cause mass peaking and upwelling below the surface of the same {N,n}o orbit shell but at high latitude region, and generates an effective equatorial slow flow stream at the surface. This (equivalent) slow flow stream also gets narrower and shallower, and eventually diminished. This single model has been used to explain the sunspot drift on Sun's surface, the continental drift on Earth surface, and both Sun's and Earth's magnetic dynamo. The alternation between two phases of Y*lm* cycle not only alternates the orientation of Sun's (or Earth's) magnetic field, but also supports the supercontinent cycle model. Under this model, the apparent random drift of post-Pangaea continents can be nicely depicted as an expected hydrodynamic result of a broken dam through a mouth located near the south end of South America continent. In papers of SunQM-3s6, SunQM-3s7, and SunQM-3s8, I used radial wave function R(*nl*) to predict the mass density r-distribution for all planets and Sun, plus the QM structure evolution for rocky planets and Sun. In papers of SunQM-3s3 and SunQM-3s9, I used spherical wave function Y(*lm*) to explain planets' and Sun's atmosphere movement, surface (or mantle) movement, and internal mass movement. Therefore, results from all these papers reveal that for all planets and stars, not only they were formed and evolved under planet's (or star's) QM, but the current movement of their internal mass is also determined by the planet's (or star's) QM.

Introduction

A series of my previous papers has shown that the formation of Solar system (and each planet-moon system) was governed by its {N,n} QM [1] ~ {12]. In papers SunQM-3s6, -3s7, and -3s8, I showed that the formation of planet's and star's (radial) internal structure is governed by the planet's or star's radial QM. In paper SunQM-3s3, I showed that the surface mass (atmosphere) movement of Jupiter (and Saturn, Earth, etc.) is governed by Jupiter (or Saturn, Earth) planet's θφ-2D dimension QM. In current paper, I'd like to further demonstrate that the internal mass movement of the current Sun and planets is also governed by their {N,n} QM. Among many properties that are known to be caused by Sun's (or planet's) internal mass movement, I choose sunspot drift, continental drift, Sun's magnetic field, and Earth's magnetic field as four examples, to show that all four phenomena can be explained under a single {N,n} QM mechanism. Note: for |n*l*m> state, if n, *l*, m are single digital, then I write |n*l*m> without comma (like |211>), if anyone is double digital, then I write it with comma (like |12,11,11>). Note: Microsoft Excel's number format is often used in this paper, for example: x^2 = x^2, 3.4E+12 = 3.4×10^{12}, 5.6E-9 = 5.6×10^{-9}.

I. Sunspot drift explained with {N,n} QM model

So far the leading model for both sunspot drift and Sun's magnetic field is Babcock's magnetic dynamo model [13]. My {N,n} QM explanation of sunspot drift is also largely based on Babcock's magnetic dynamo model.

I-a. "Y*lm* cycle" model

From previous papers, we know that Sun's {0,1}o orbit shell space (from Sun core's surface to Sun's surface) can be described by a number of (slightly) different QM states:
1) {0,1//6}o orbit shell (with Sun core {0,1//6} as r_1). So it is mainly in |100> state and partly in |2*l*m> state, with wave function ψ(1,0,0) + ψ(2,*l*,m), where the effective ψ(2,*l*,m) ≈ ψ(2,1,1), (see paper SunQM-3s3 for explanation).
2) {-1,n=6..11//6}o orbit shells (with Sun's {-1,1//6} as r_1). So it is in |11,*l*,m> states, with wave functions Σ [ψ(n,*l*,m)], where n=6 to 12, and the effective ψ(12,*l*,m) ≈ ψ(12,11,11).
3) {0,1//2}o orbit shell (with Sun core {0,1//6} as r_1). So it is mainly in |100> state and partly in |2*l*m> state, with wave function ψ(1,0,0) + ψ(2,*l*,m), where the effective ψ(2,*l*,m) ≈ ψ(2,1,1).
4) {-1,n=2..3//4}o orbit shells, with Sun's "metallic" core (made of atoms heavier than He, see paper SunQM-3s8) {-1,3//6} as r_1. So it is in |2*l*m>, |3*l*m>, and |4*l*m> ≈ |433> states, with wave functions Σ [ψ(n,*l*,m)], where n=1 to 4.

Although {-1,n=6..11}o QM mode gives a more accurate description for sunspot drifting, it is too complicated to plot out for explanation. To simplify the explanation, here I use the combination of {0,1//2}o and {-1,n=2..3//4}o QM modes for the QM explanation of sunspot drift.

From previous papers, we know that the Solar {N,n} QM structure can be described by the Schrodinger equation and solution, i.e., the wave function, in a integration form:

$$\iiint |\Psi_{nlm}|^2 r^2 \sin(\theta)\, dr\, d\theta\, d\varphi = \iiint |Rnl|^2 \, |Ylm|^2 r^2 \sin(\theta)\, dr\, d\theta\, d\varphi,$$

From paper SunQM-3s6 through SunQM-3s8, we know that for a {-1,n=1..3//4}o QM modeled Sun, its mass distribution can be described by the integration equation:

$$\text{Mass}(r, \theta, \varphi) = \iiint r^2 * [(|R(1,0)|^2 + |R(2,l)|^2 + |R(3,l)|^2 + |R(4,l)|^2)]_{\{-1,n=1..3\}o} * W * D * \sin(\theta) * r^2\, dr\, d\theta\, d\varphi, \; [r=0, 6.96E+8 \text{ m}; \theta=0, \pi; \varphi=0, 2\pi]$$

where D(r, θ, φ) is the mass density distribution, and W is a scaling factor.

In paper SunQM-3s3 Figure 3, I used θφ-2D-dimension wave function and probability distribution sin(θ)*|Y(*l*,m)|^2 to model out Jupiter's atmospheric surface pattern. Now I am going to use the similar θφ-2D-dimension probability distribution |Y(*l*,m)|^2 to model out sunspot drift's butterfly pattern at Sun surface. Figure 1 shows the plot of |Y(*l*,m)|^2 vs. θ for *l* (= m) = 1, 2, 3, 11, and 71. The calculation of Figure 1 is shown in Table 1. Note: in Table1 and Figure 1, to make |211> band's edge at +/- 30° latitude, I have to adjust the factor to 0.4 (see column 5 of Table 1).

For a good model to explain the sunspot drift, it needs not only to explain the butterfly pattern, but also to satisfy the Hale's observation result (see section I-d). Plus, this model should be consistent with the explanation of Sun's other major properties (like Sun's magnetic field, etc.). Furthermore, if the same model can be used to explain Earth's continent drift and magnetic field, then this model will have much better chance to be a correct one. Mainly based on the sunspot's butterfly pattern, also combined Babcock's magnetic dynamo and Earth's magnetic field dynamo model (see wiki "Earth's magnetic field"), I build a new model by completely using {N,n} QM model to explain all above phenomena. I named this model as "Y*lm* cycle" model (or Y*lm* cycle effect). The "Y*lm* cycle" model has two phases, Phase-1 is explained in Figure 1, and phase-2 is explained in Figure 2.

Table 1. Plot of |Y(*l*,m)|^2 vs. θ for *l* = 1, 2, 3, and *l* (= m) = 11, and 71.

θ, in π	θ, in arc	θ', in degree	3D projected to 2D y=sin(θ')= cos(θ)	spin caused y=sin(θ'*0.4) 0.4	|Y(0,0)|^2	|Y(1,0)|^2	|Y(1,±1)|^2	|Y(2,0)|^2	|Y(2,±1)|^2	|Y(2,±2)|^2	|Y(3,0)|^2	|Y(3,±1)|^2	|Y(3,±2)|^2	|Y(3,±3)|^2	|Y(11,±11)|^2	|Y(71,±71)|^2
0	0	90	1	0.5878	7.96E-02	2.39E-01	0.00E+00	3.98E-01	0.00E+00	0.00E+00	5.57E-01	0.00E+00	0.00E+00	0.00E+00	0.00E+00	0.00E+00
1/32	0.098	84	0.995	0.5556	7.96E-02	2.36E-01	2.29E-03	3.87E-01	1.14E-02	2.75E-05	5.26E-01	3.13E-02	1.91E-04	3.09E-07	3.96E-23	8.85E-144
1/16	0.196	79	0.981	0.5225	7.96E-02	2.30E-01	9.09E-03	3.54E-01	4.37E-02	4.32E-04	4.39E-01	1.15E-01	2.91E-03	1.92E-05	1.49E-16	2.49E-101
3/32	0.295	73	0.957	0.4886	7.96E-02	2.19E-01	2.01E-02	3.04E-01	9.21E-02	2.12E-03	3.18E-01	2.25E-01	1.36E-02	2.08E-04	9.36E-13	8.00E-77
1/8	0.393	68	0.924	0.4540	7.96E-02	2.04E-01	3.50E-02	2.42E-01	1.49E-01	6.40E-03	1.91E-01	3.27E-01	3.82E-02	1.09E-03	4.09E-10	8.82E-60
5/32	0.491	62	0.882	0.4187	7.96E-02	1.86E-01	5.30E-02	1.77E-01	2.06E-01	1.47E-02	8.56E-02	3.87E-01	8.02E-02	3.82E-03	4.02E-08	6.35E-47
3/16	0.589	56	0.831	0.3827	7.96E-02	1.65E-01	7.37E-02	1.15E-01	2.55E-01	2.84E-02	2.01E-02	3.89E-01	1.38E-01	1.02E-02	1.49E-06	8.61E-37
7/32	0.687	51	0.773	0.3461	7.96E-02	1.43E-01	9.61E-02	6.25E-02	2.87E-01	4.83E-02	1.25E-05	3.32E-01	2.02E-01	2.27E-02	2.76E-05	1.31E-28
1/4	0.785	45	0.707	0.3090	7.96E-02	1.19E-01	1.19E-01	2.49E-02	2.98E-01	7.46E-02	1.74E-02	2.35E-01	2.61E-01	4.35E-02	3.01E-04	6.44E-22
9/32	0.884	39	0.634	0.2714	7.96E-02	9.61E-02	1.43E-01	4.28E-03	2.87E-01	1.07E-01	5.47E-02	1.28E-01	3.00E-01	7.43E-02	2.14E-03	2.02E-16
5/16	0.982	34	0.556	0.2334	7.96E-02	7.37E-02	1.65E-01	5.45E-04	2.55E-01	1.43E-01	9.12E-02	4.26E-02	3.08E-01	1.15E-01	1.06E-02	6.32E-12
11/32	1.080	28	0.471	0.1951	7.96E-02	5.30E-02	1.86E-01	1.11E-02	2.06E-01	1.81E-01	1.10E-01	2.00E-03	2.81E-01	1.64E-01	3.88E-02	2.71E-08
3/8	1.178	23	0.383	0.1564	7.96E-02	3.50E-02	2.04E-01	3.13E-02	1.49E-01	2.17E-01	1.05E-01	1.28E-02	2.23E-01	2.17E-01	1.08E-01	1.99E-05
13/32	1.276	17	0.290	0.1175	7.96E-02	2.01E-02	2.19E-01	5.55E-02	9.21E-02	2.50E-01	7.80E-02	6.41E-02	1.48E-01	2.67E-01	2.34E-01	2.94E-03
7/16	1.374	11	0.195	0.0785	7.96E-02	9.09E-03	2.30E-01	7.81E-02	4.37E-02	2.76E-01	4.18E-02	1.32E-01	7.36E-02	3.10E-01	4.02E-01	9.68E-02
15/32	1.473	6	0.098	0.0393	7.96E-02	2.29E-03	2.36E-01	9.38E-02	1.14E-02	2.93E-01	1.17E-02	1.87E-01	1.97E-02	3.38E-01	5.54E-01	7.67E-01
31/64	1.522	3	0.049	0.0196	7.96E-02	5.75E-04	2.38E-01	9.80E-02	2.87E-03	2.97E-01	2.99E-03	2.03E-01	5.01E-03	3.46E-01	6.00E-01	1.28E+00
32/65	1.546	1	0.025	0.0098	7.96E-02	1.44E-04	2.39E-01	9.91E-02	7.18E-04	2.98E-01	7.53E-04	2.08E-01	1.26E-03	3.48E-01	6.12E-01	1.46E+00
1/2	1.571	0	0	0	7.96E-02	8.96E-34	2.39E-01	9.95E-02	4.48E-33	2.98E-01	4.70E-33	2.09E-01	7.84E-33	3.48E-01	6.16E-01	1.52E+00
33/65	1.595	-1	-0.025	-0.0098	7.96E-02	1.44E-04	2.39E-01	9.91E-02	7.18E-04	2.98E-01	7.53E-04	2.08E-01	1.26E-03	3.48E-01	6.12E-01	1.46E+00
33/64	1.620	-3	-0.049	-0.0196	7.96E-02	5.75E-04	2.38E-01	9.80E-02	2.87E-03	2.97E-01	2.99E-03	2.03E-01	5.01E-03	3.46E-01	6.00E-01	1.28E+00
17/32	1.669	-6	-0.098	-0.0393	7.96E-02	2.29E-03	2.36E-01	9.38E-02	1.14E-02	2.93E-01	1.17E-02	1.87E-01	1.97E-02	3.38E-01	5.54E-01	7.67E-01
9/16	1.767	-11	-0.195	-0.0785	7.96E-02	9.09E-03	2.30E-01	7.81E-02	4.37E-02	2.76E-01	4.18E-02	1.32E-01	7.36E-02	3.10E-01	4.02E-01	9.68E-02
19/32	1.865	-17	-0.290	-0.1175	7.96E-02	2.01E-02	2.19E-01	5.55E-02	9.21E-02	2.50E-01	7.80E-02	6.41E-02	1.48E-01	2.67E-01	2.34E-01	2.94E-03
5/8	1.963	-23	-0.383	-0.1564	7.96E-02	3.50E-02	2.04E-01	3.13E-02	1.49E-01	2.17E-01	1.05E-01	1.28E-02	2.23E-01	2.17E-01	1.08E-01	1.99E-05
21/32	2.062	-28	-0.471	-0.1951	7.96E-02	5.30E-02	1.86E-01	1.11E-02	2.06E-01	1.81E-01	1.10E-01	2.00E-03	2.81E-01	1.64E-01	3.88E-02	2.71E-08
11/16	2.160	-34	-0.556	-0.2334	7.96E-02	7.37E-02	1.65E-01	5.45E-04	2.55E-01	1.43E-01	9.12E-02	4.26E-02	3.08E-01	1.15E-01	1.06E-02	6.32E-12
23/32	2.258	-39	-0.634	-0.2714	7.96E-02	9.61E-02	1.43E-01	4.28E-03	2.87E-01	1.07E-01	5.47E-02	1.28E-01	3.00E-01	7.43E-02	2.14E-03	2.02E-16
3/4	2.356	-45	-0.707	-0.3090	7.96E-02	1.19E-01	1.19E-01	2.49E-02	2.98E-01	7.46E-02	1.74E-02	2.35E-01	2.61E-01	4.35E-02	3.01E-04	6.44E-22
25/32	2.454	-51	-0.773	-0.3461	7.96E-02	1.43E-01	9.61E-02	6.25E-02	2.87E-01	4.83E-02	1.25E-05	3.32E-01	2.02E-01	2.27E-02	2.76E-05	1.31E-28
13/16	2.553	-56	-0.831	-0.3827	7.96E-02	1.65E-01	7.37E-02	1.15E-01	2.55E-01	2.84E-02	2.01E-02	3.89E-01	1.38E-01	1.02E-02	1.49E-06	8.61E-37
27/32	2.651	-62	-0.882	-0.4187	7.96E-02	1.86E-01	5.30E-02	1.77E-01	2.06E-01	1.47E-02	8.56E-02	3.87E-01	8.02E-02	3.82E-03	4.02E-08	6.35E-47
7/8	2.749	-68	-0.924	-0.4540	7.96E-02	2.04E-01	3.50E-02	2.42E-01	1.49E-01	6.40E-03	1.91E-01	3.27E-01	3.82E-02	1.09E-03	4.09E-10	8.82E-60
29/32	2.847	-73	-0.957	-0.4886	7.96E-02	2.19E-01	2.01E-02	3.04E-01	9.21E-02	2.12E-03	3.18E-01	2.25E-01	1.36E-02	2.08E-04	9.36E-13	8.00E-77
15/16	2.945	-79	-0.981	-0.5225	7.96E-02	2.30E-01	9.09E-03	3.54E-01	4.37E-02	4.32E-04	4.39E-01	1.15E-01	2.91E-03	1.92E-05	1.49E-16	2.49E-101
31/32	3.043	-84	-0.995	-0.5556	7.96E-02	2.36E-01	2.29E-03	3.87E-01	1.14E-02	2.75E-05	5.26E-01	3.13E-02	1.91E-04	3.09E-07	3.96E-23	8.85E-144
1	3.142	-90	-1	-0.5878	7.96E-02	2.39E-01	3.58E-33	3.98E-01	1.79E-32	6.72E-65	5.57E-01	5.02E-32	4.71E-64	1.18E-96	0.00E+00	0.00E+00

Note: |Y(11,±11)|^2, and |Y(71,±71)|^2 are calculated according to John S. Townsed, A Modern Approach to Quantum Mechanics, 2nd ed., 2012. Page 334, formula 9.146, Y(*l*,*l*) = (-1)^*l* /2^*l* /*l*! sqrt[(2*l* +1)! /(4π)] * exp(i*l*φ) * [sin(θ)]^*l* .

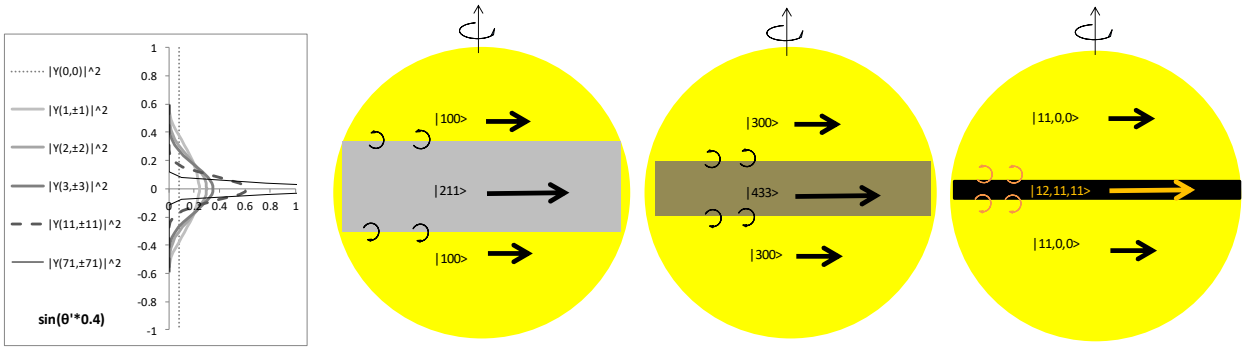

Figure 1 (from left to right: a, b, c, and d). Y*lm* cycle model. Phase-1 of sunspot drift is caused by a series of (near surface) nLL convections evolving from |211> state to |322>, |433>, |544>, … |12,11,11>, |72,71,71>, and probably even higher |nLL> states.

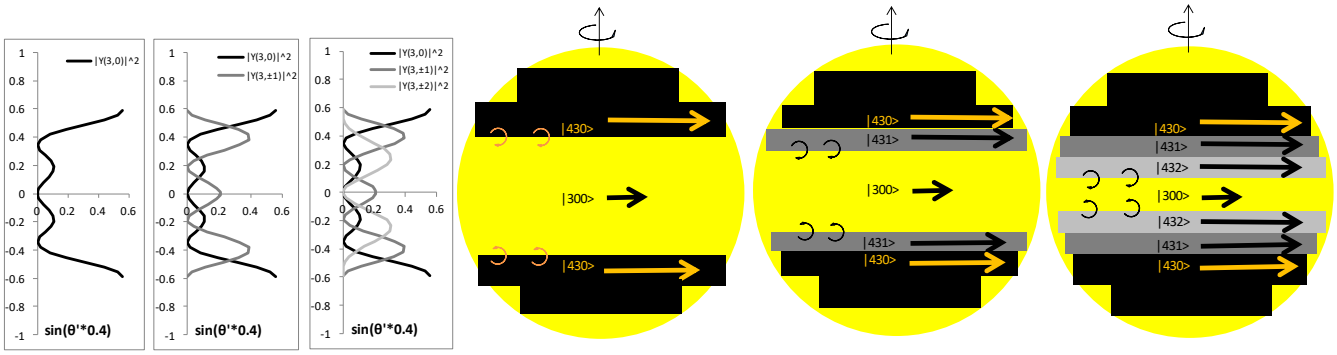

Figure 2 (from left to right: a, b, c, d, e, and f). Y*lm* cycle model. Phase-2 of sunspot drift can be simplified as it is caused by a series of (near surface) nLm convections evolving from |430>, to |4,3,m=0..1>, and then to |4,3,m=0..2>. Here I use an easy to understand way to present the diagram: using |n*l*m> with n=4 only: In Figure 2d, between around +/- 30° region is the slower |300> state, both above +30° and below -30° regions are the faster |430> state; In Figure 2e, between around +/- 20° region is the slower |300> state, both above +20° and below -20° regions are the faster |43m> state, where m = 0..1; In Figure 2f, between around +/- 10° region is the slower |300> state, both above +10° and below -10° regions are the faster |43m> state, where m = 0..2.

Another way to present phase-2's Y*lm* cycle diagram (less easy to understand, but more accurate, and completely symmetric to Figure 1b, 1c, 1d) is: In Figure 2d, between around +/- 30° region is the slower |100> state, both above +30° and below -30° regions are the faster |210> state; In Figure 2e, between around +/- 20° region is the slower |300> state, both above +20° and below -20° regions are the faster |43m> state, where m = 0..2; In Figure 2f, between around +/- 10° region is the slower |11,0,0> state, both above +10° and below -10° regions are the faster |12,11,m> state, where m = 0..10.

I-b. "Y*lm* cycle" model phase-1 explanation

The initial state is the |n00> state on Sun surface, here we choose |100> state. The phase-1 of sunspot drift is caused by a series of (near surface) nLL convections evolving from |211> state to |322>, |433>, |544>, … |12,11,11>, |72,71,71>, and probably to even higher |nLL> states (see Figure 1a). The |nLL> convection idea comes from the QM explanation of Jupiter atmospheric equatorial zonal band |544> (see paper SunQM-3s3), where a QM mass peaking effect at 1.4E+6 m below the equatorial surface pushes (or convects) the mass to the surface, and forms Jupiter's equatorial zonal band |544> at eastward speed ~125 m/s faster than the neighboring belt bands. The major difference between Jupiter's equatorial zonal band and Sun's sunspot pair is that one (apparently) keeps the |544> constantly, and another evolves from |211> to |433>, then to higher |nLL>, so its band width become narrower and eventually diminishes (see Figure 1b, 1c, 1d). Here I name this Y*lm* cycle phase-1 sunspot related |nLL> band as "sunspot zonal band".

So the QM state |n*l*m> that dominating the sunspot drift is not the |0,1//2}o orbit space's n=1 or |100> state (with Sun core {0,1//6} as r_1), but the surface embedded |211> state; or not the |0,3//4}o orbit space's n=3 or |300> state, but the surface embedded |433> state; or not the |-1,11//6}o orbit space's n=11 or |11,0,0> state, but the surface embedded |12,11,11> state. Therefore, in Figure 1, I show the probability densities of |Y(1,1)|^2, |Y(3,3)|^2, |Y(11,11)|^2, etc. |Y(71,71)|^2 in Figure 1 is for n=72, or |72,71,71> state, which is the multiplier n' of |2,1,1> at 2*6*6. In other words, in the Y*lm* cycle model, the |n-1,0,0> state (because its Y(0,0) is spherical) forms the Sun's (background) surface shell with slow eastward spin speed, while the fast eastward spin sunspot zonal band is a |nLL> state embedded in the slow spinning |n-1,0,0> state formed background spherical shell surface. For better understanding, please see Figure 4 in paper SunQM-3s3, and also see [13].

At the interface between the fast eastward moving |nLL> zonal band and the slow eastward moving |n-1,0,0> background spherical shell, many turbulent swirls are formed (see wiki "Jupiter" figure "*Time-lapse sequence from the approach of Voyager 1*" as example). I believe that these swirls are the origin of sunspots (see many small swirls in Figure

1b, 1c, and 1d). So the sunspots are the marks of the edge of the |nLL> zonal band, and the butterfly pattern of the sunspot pairs reveals that |nLL> zonal band getting narrower from the early phase to the later phase in phase-1 of Y*lm* cycle. From this model, we can estimate the depth of the QM mass peaking site beneath the Sun surface (for sunspot zonal band).

I-c. The origin (or the depth) of the QM mass peaking effect for the convection of Y*lm* cycle (phase-1)

I believe the origin of the Y*lm* cycle effect comes from the convection. From paper SunQM-3s8, Table 2, Sun's {0,1//6}o orbit space can be further divided into {-1,n=6..11}o orbit shells. Among them, only two outmost orbit shells {-1,n=10..11}o (from 69%R to 84%R, and from 84%R to 100%R) are currently in convection state. So the origin of the Y*lm* cycle effect must comes from one of them.

If we have known the sunspot zonal band's speed relative to the background (like that of Jupiter zonal band's wind speed), then we can calculated out how deep the convection started (like paper SunQM-3s3 Table 3's calculation for Jupiter surface's zonal band). Before doing that, we need first to know what x value we should use for the Sun's internal Spin-Reference-Frame (SpnRefFrm, $\omega_{n\text{-}spin} = \omega_{1\text{-}spin} / n\text{^}x$, x from 0 to 4. See paper SunQM-3s1).

Wiki "Solar rotation" (or wiki "Differential rotation") figure "*Internal rotation in the Sun*" shows Sun's internal spin speed (modeled from the helioseismology data) [14]. This figure is represented in the current paper as Figure 3a. Figure 3b shows a simplified version for Figure 3a. Figure 3a reveals that Sun surface's spin speed significantly decreases at r > ~95%R (note: %R means % of Sun radius). Considering that to form a fast eastward moving zonal band through convection, Sun inner shell's (eastward) spin speed must be significantly faster than that of the outer (or the surface) shell, so the origin of the sunspot convection point must be at the outer edge of the {-1,11}o orbit shell, or in the radius region between 95%R to 100%R.

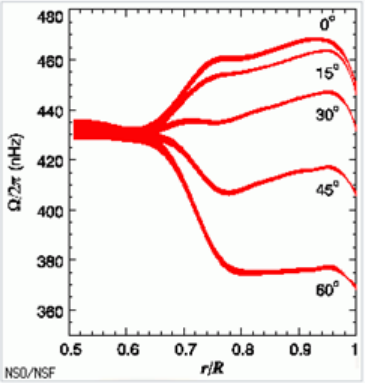

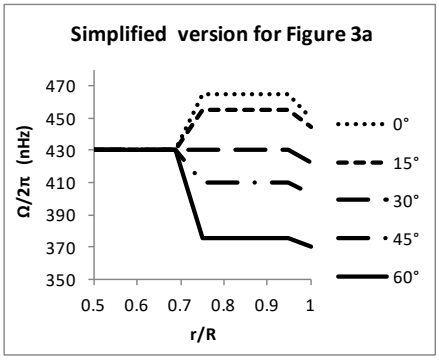

Figure 3a (left). Internal rotation in the Sun. Copied from Wiki "Solar rotation", figure "*Internal rotation in the Sun*". Copy right: CC BY-SA 3.0. Author: Global Oscillation Network Group [14].
Figure 3b (right). Simplified version for Figure 3a. It will be used to explain Sun's magnetic dynamo in section II.

Using data in Figure 3a, we can estimate the x value for SpnRefFrm's $\omega_{n\text{-}spin} = \omega_{1\text{-}spin} / n\text{^}x$. To do this, I constructed Table 2. Columns 2 and 3 in Table 2 are Sun's spin speed in nHz (read out directly from Figure 3a) at different latitude, and at 98%R or 100%R. In columns 4 and 5, the speed of nHz is transformed into m/s (for example v = 2π*0.98*6.96E+8 *(461 nHz) * 1E-9 = 1975.7 m/s). The relationship of x to 98%R, 100%R, and v at 98%R, 100%R is deduced as follows (define $r_n > r_1$): $\omega_{n\text{-}spin} = \omega_{1\text{-}spin} / n\text{^}x$, $n\text{^}x = \omega_1 / \omega_n$, $n = (r_n/r_1)\text{^}(1/2)$, $\omega_n = v_n / r_n$, $(r_n/r_1)\text{^}(x/2) = (v_1/r_1) / (v_n/r_n)$, $(r_n/r_1)\text{^}(x/2\text{-}1) = (v_1/v_n)$, $(r_1/r_n)\text{^}(1\text{-}x/2) = (v_1/v_n)$, $(1\text{-}x/2) \log(r_1/r_n) = \log(v_1/v_n)$, or $x = 2*[1- \log(v_1/v_n) / \log(r_1/r_n)]$. Column 7 of Table 2 shows that the calculated x = 2.39 at 0 degree, and x = 1.33 at 60 degree latitude. So within the data error range, x is between 2.4 (at equator) to 1.3 (near poles).

Table 2. Estimate x value for $\omega_{n\text{-spin}} = \omega_{1\text{-spin}} / n^{\wedge}x$ between 98%R to 100%R according to Figure 3a.

r (meter)			6.82E+08	6.96E+08		
latitude	nHz at 98%R	nHz at 100%R	98%R spin speed	100%R spin speed	Δ(spin speed) /Δ(2%R)	x= 2*[1-log(v_1/v_n) / log(r_1/r_n)]
degree	nHz	nHz	m/s	m/s	(m/s) /(m/m)	
0	461	450	1975.7	1967.9	7.8	2.39
15	458	447	1962.8	1954.8	8.0	2.41
30	443	433	1898.5	1893.6	5.0	2.26
45	414	406	1774.3	1775.5	-1.2	1.93
60	374	369	1602.8	1613.7	-10.8	1.33

Now we can estimate the depth of the mass convection. The column 6 of Table 2 shows that at equatorial region, an upwelling mass from 98%R to 100%R will cause the zonal band moving eastward ~ 8 m/s faster. Considering Sun's internal spin speed maximized at ~95%R (at all latitudes, see Figure 3a), the most reasonable explanation is that the sunspot zonal band is formed by convection started at around 95%R (or around 5% * 6.96E+8 = 3.48E+7 m beneath the Sun surface, from 0° to +/-30°). So in this model, a mass peaking and upwelling at 95%R of Sun will generate (a mean value of) ~ 20 m/s faster zonal band (to the eastward or +φ direction) at Sun surface. The sunspots (which are the turbulent swirls at the edge of the zonal band) should not move faster than that. However, wiki "Sunspot" mentions that sunspots "*may travel at relative speeds, or proper motions, of a few hundred meters per second when they first emerge*" (here I believe that sunspots move in eastward, the same direction of Sun spin). So I guess that "a few hundred meters per second" mentioned from wiki must be some extreme cases where the speed is at least 1σ above the mean value in the normal distribution of sunspot speed (see more explanation later).

I believe that the |211> convection may have a (relative) deeper origin than that of the |12,11,11> convection. For example, in Figure 3a, instead of maximized constantly at ~95%R, Sun's internal spin speed maximum may be at ~93%R at early phase-1 (when |211> mode is dominant), and at ~98%R at the later phase-1 (when |12,11,11> is dominant). So that the origin of the mass peaking and upwelling is at ~93%R at early phase-1 (when |211> mode is dominant), and at ~98%R at the later phase-1 (when |12,11,11> is dominant). Because Figure 3a is presented as the average of 22 years, it lost the time-dependent information. So if the Figure 3a can be re-presented in 22 figures (rather than in one figure), and each figure presents one year's averaged data, then we will be able to see the difference between phase-1 and phase-2, and also the difference between early and later stage of each phase. Besides that, Figure 3a's helioseismology data need also to be measured and modeled according to Y*lm* cycle model's |nLL> zonal band shape. For example, in phase-1, it should model the sunspot zonal band (between sunspot pair, which gradually narrowing from +/- 30° to ~0°) as one quanta, and rest part as another quanta. Especially the data between 30° to 5° latitude has to been presented in each detailed time frame, rather than averaged over all time during phase-1 (or even averaged with phase-2). Once the Figure 3a's helioseismology data is remodeled and represented, I believe the |nLL> zonal band model analysis will give much clear cut result.

From paper SunQM-3s1, we know that for < 1% mass occupancy space, nLL effect changes the mass distribution from a sphere to a disk. One thing I learned from the Y*lm* cycle phase-1 analysis is that **for ~ 100% mass occupancy at convective zone, nLL effect seems disk-lyze the RF velocities (not the particles themselves, but the velocity vectors those particles carry)! It disk-lyze the high end of Boltzmann velocity distribution's velocity vectors (which is in RF) into nLL disk. I name it as "nLL disk-lyze velocity vector" effect**. This causes the zonal band become narrower and narrower as well as shallower and shallower, while its east moving speed become faster and faster. If this is correct, then it can explain why some of sunspots can move fast at "a few hundred meters per second" as wiki mentioned. However, I need to use math to check whether this idea is correct or not (just like what I did in paper SunQM-3s1 for 1% mass occupancy's mass nLL disk-lyzation).

If Y*lm* cycle phase-1 caused |nLL> zonal band is ~20 m/s faster than the background |n-1,0,0> shell, then in the Sun spinning frame (or suppose Sun does not spin), after 11 years of phase-1, the zonal band will travel (20*11*365*24*3600 =) 6.94E+9 m, or about 1.6 rounds around Sun. If the |nLL> zonal band is ~100 m/s faster than the background |n-1,0,0> shell, then it will travel about 8 rounds around Sun during 11 years of phase-1.

I-d. Explanation of Hale's phenomenon (in phase-1 of Y*lm* cycle)

Hale's observation on sunspot (as shown in Neil F. Comins & William J. Kaufmann's book [13] pp327): "… *below the photosphere, the gases that surround each sunspot whip around like hurricanes as large as Earth's diameter … on one hemisphere of the Sun, sunspots with a magnetic north pole always come into view before the corresponding sunspots with a magnetic south pole. At the same time at the other hemisphere, the order is reversed. … this patter reverses about itself about 11 years. The hemisphere where north magnetic poles come first during one 11-year cycle has south magnetic pole coming first during the next*". From wiki "sunspot", "*Sunspots usually appear in pairs of opposite magnetic polarity*".

According to these observations, and by comparing to Jupiter atmosphere band pattern, I believe that the turbulent swirls at the interface between the fast eastward zonal band and slower eastward belt band (in both phase-1 and phase-2 of Y*lm* cycle) are the origins of sunspots. Figure 4a shows the detailed explanation. At +30° latitude, the speed difference between the fast eastward |211> zonal band and the slower eastward |100> background induces anti-clock major local swirls (see dark-green spiral arrows in Figure 4a) at the interface, forming (right-hand) magnetic N pole, and causing magnetic line shooting out of Sun surface. The sharp front of anti-clock major local swirls induces the secondary clock-wise minor local swirls (see light-green spiral arrows in Figure 4a), forming (right-hand) magnetic S pole, causing magnetic line piercing back into Sun surface. These magnetic N and S poles forms pairs, and generate local and cross equator corona loops (see red arrows in Figure 4a, and also see NASA's video picture at Figure 4b). (Notice that the definition of S-pole and N-pole on Sun surface is opposite to that in book [13]). At -30° latitude, the same thing happens, but with the opposite direction of swirling. Those super large major local swirls are the (visible) sunspots emerged at +/- 30° latitude. As the zonal band evolves to higher n of |nLL> state, the zonal band width becomes narrower, therefore it forms the butterfly patterned sunspots pairs in phase-1 of Y*lm* cycle. At the end of phase-1, the Y*lm* regresses back to the |n00> state (or |100> state).

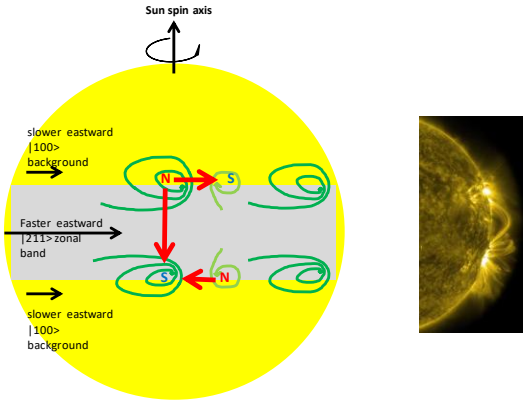

Figure 4a. Speed differential induced turbulent swirls cause sunspots, and coronal loops.
Figure 4b. Picture copied from wiki "coronal loop", video "coronal loop" at 0:22/1:41 , Author: NASA/Goddard Space Flight Center. Copy right: public domain.

I-e. Y*lm* cycle model phase-2 explanation

While the explanation of Phase-1 is directly based on both the sunspot's butterfly pattern and Babcock's magnetic dynamo model, the explanation of Phase-2 is based only on the sunspot's butterfly pattern, and not on the Babcock's model (because I don't understand how it can explain phase-2). In Figure 2, I try to use |4*l*m> states to explain the phase-2 of Y*lm* cycle model. Although it is less accurate, it is much easier for explanation as well as for understanding. Again the initial state on the Sun surface is |n00> state, here we choose |300> state (only for the explanation of |4*l*m> states caused convection). First, the |430> state gradually forms on top of the |300> background state on Sun surface in regions of +30° to +90° (and -

30° to -90°), and causes the new convection which makes eastward spin faster (than that without convection) in these two surface regions.

At the interface around +30° latitude, the |430> band is moving ~20 m/s faster than that of |300> band, causing many clock-wise major local swirls (see many small swirls in Figure 2d), and they form sunspots with (the right hand) magnetic S pole. As phase-2 evolves, the |431> state gradually forms (and join with the |430> state) on top of the |300> background state on Sun surface in regions between +20° to +30° (and -20° to -30°), causing the new convection which makes eastward spin ~20 m/s faster than that without convection in these two regions. It also causes the eastward sunspots drift shifting from +/- 30° to +/- 20°. As phase-2 further evolves, the |432> state gradually forms on top of the |300> background state on Sun surface in regions between +10° to +20° (and -10° to -20°). Again, this causes sunspot drift shifting from around +/- 20° to around +/- 10° latitude. At the end of phase-2, the Y*lm* again regresses back to the |n00> state (or |300>, or |100> state). In this way it forms phase-2's sunspot butterfly pattern. Readers can figure out the Hale observation effect for your own, just remember that the directions of swirls are exactly opposite as those in phase-1.

Notice that while phase-1 zonal band is a true zonal band, the phase-2's slower equatorial band act as an effective belt band (see paper SunQM-3s3 for belt band). So I name this Y*lm* cycle phase-2 sunspot related |n,L,m=0..L-1> band as "sunspot belt band". Just like that of the sunspot zonal band in phase-1, this sunspot belt band in phase-2 also gets narrower and shallower (and maybe slower?), and eventually diminished.

I-f. The driving force to onset phase-1 or phase-2 of Y*lm* cycle

In Table 1 and Figure 1, to make |211> band's edge to be at around +/- 30° latitude (where sunspots emerge in the early phase-1), I have to adjust the factor to 0.4 (see column 5 of Table 1). Comparing to the same factor values of Jupiter (x0.7), Saturn (x0.7) and Earth (x0.9), the factor value of Sun's (x0.4) is very low. Although Sun's larger radius makes some contribution to this very low value, I believe that the main reason comes from that the mass density at Sun surface (where the convection starts) is much lower than that at the Jupiter surface. Therefore the centrifugal force's tangential component (see paper SunQM-3s1 Figure 2 right) is much easier to drive the low density mass (gas) on Sun surface to the equator region. The supportive data can be seen in a Table of "*Surface Pressure of the Planets and the Sun (Source: NASA)*" from website "http://www.smartconversion.com/otherInfo/Surface_pressure_of_planets_and_the_sun.aspx" (data not shown here).

The evolution of sunspot zonal band |nLL> mode in phase-1 from low n to high n (see Figure 1a) must come from that the convective site is relatively deeper at beginning, then moves to less deep. Eventually the convection origin becomes too shallow to sustain itself (and zonal band become too narrow to exist), so this convection dies, and it ends the phase-1. Therefore, this Y*lm* convection mode is independent to the general convection mode in most part of Sun's {-1,n=10..11}o orbit space (or from ~69%R to ~95%R). For phase-2, it is expected that the convection also starts from relative deeper layer then moves to shallower layer.

The driving force to onset phase-1, or to form Y*lm* cycle's |nLL> zonal band is easy to understand: it comes from Sun QM's nLL disk-lyzation effect. The QM mass peaking effect causes the convection at around 95%R near the Sun surface. The very low mass density at Sun surface causes the nLL disk-lyzing effect to form the true disk at the equator of Sun surface. So at the end of phase-1, significant amount of surface mass is pulled out from the high latitude region and piled up near the equator of Sun surface. Because of this, at the end of phase-1, Sun may lumped out at equator region (even the absolute mass density of the lump is still very low). Also the "nLL disk-lyze velocity vector" effect may form the very fast moving |nLL> zonal band with ~100 m/s (relative) speed.

The driving force to onset phase-2 of Sun's Y*lm* cycle is less clear. One possible hypothesis is: at the later stage of phase-1, the surface (r > 98%R) mass at high latitude region (from +30° and up or -30° and down) is mostly depleted, so that the mass underneath of this region has to expand upward because of the less gravity pressure on top of it. For example, the mass at layer from 95%R to 96%R now expand to from 96%R to 98%R (remember this is only at regions from +30° and up or -30° and down, not equator region, and this is not driven by QM, but by gravity, or by gas pressure). The faster eastward spin speed from the 95%R now is carried over by expanded mass to 98%R. This mushroom shaped faster spin pattern looks exactly like the |210> probability density pattern (see book David J. Griffiths, Introduction to Quantum Mechanics, 2nd ed., 2015, pp159, Figure 4.6. $|\psi_{210}|^2$, and $|\psi_{310}|^2$). This triggers the onset of |210> QM mode for Sun, therefore starts the phase-2

of Sun's Y*lm* cycle. As |210> mode's QM force peaking the mass at high latitude region, it depletes mass from the neighboring region (between +30˚ to +20˚ , or -30˚ to -20˚ latitude). Then the mass at layer from 95%R to 96%R in these two regions also expand to from 96%R to 98%R (again not by QM mass peaking effect, but by less gravity or less gas pressure), and this causes the faster spin mode evolves from |210> mode to |3,2,m=0..1> modes, |4,3,m=0..2> modes, |12,11,m=0..10>, etc., (or in Figure 2, simplified as from |430> mode to |4,3,m=0..1> modes, then to |4,3,m=0..2> modes), until the n is too high to sustain the convection. So at the end of phase-2, the lumped mass at Sun surface's equatorial region is completely shrunk.

II. Using {N,n} QM and Y*lm* cycle model to explain Sun's magnetic dynamo

From wiki "*Dynamo theory", "Dynamo theory describes the process through which a rotating, convecting, and electrically conducting fluid acts to maintain a magnetic field. This theory is used to explain the presence of anomalously long-lived magnetic fields in astrophysical bodies. The conductive fluid in the geodynamo is liquid iron in the outer core, and in the solar dynamo is ionized gas at the tachocline*".

From paper SunQM-3s8's analysis, we know that Sun's convective zone {-1,n=10..11}o orbit space covers from 69%R to 100%R. After many tries, I eventually developed one way to explain the Sun's magnetic dynamo. In this explanation, data in Figure 3a has to be simplified into three sections as shown in Figure 3b: 1) "Tachocline" zone covers 69%R to 75%R; 2) 75%R ~ 95%R convective zone, and 3) "Y*lm* cycle" zone covers 95%R to 100%R. The major simplification in Figure 3b (in comparison to Figure 3a) is that in 75%R ~ 95%R zone, the angular velocity $\Omega/(2\pi)$ is constant relative to r. The analysis shows only Tachocline zone and Y*lm* cycle zone (but not the 75%R ~ 95%R zone) make contribution to generate Sun's magnetic field. Following is the detailed explanation.

Figure 5a and Figure 6b demonstrate how the Sun's magnetic field is generated by the Tachocline zone's high latitude region. It is mostly based on the Dynamo theory with some modification (see wiki "Dynamo theory" figure "*Illustration of the dynamo mechanism that creates the Earth's magnetic field*"). Because Tachocline zone's high latitude region (+30° to +90° or -30° to -90°) has higher spin speed at the inner edge (or at 69%R) than that at outer edge (or at 75%R, see Figure 3a, or 3b), therefore, the speed differential of east-spin at 69%R and 75%R inside Sun induces many small local west-spin swirls in this shell (see Figure 5a, in top view, many local small blue westward (or clock-wise) swirls are induced).

When atoms are ionized inside the Sun, the positive ions carry almost all atoms' mass, and negative ions (electrons) carry almost zero mass. In macro-scale, both positive ions and electrons spin with Sun. In micro-scale, both positive ions and electrons are doing random movement (or at RF under Sun's QM). Here we have a big assumption: the driving forces of both convection and Y*lm* cycle only affect the positive ions because they have (relative) large mass, and these driving forces do not affect electrons because they have almost zero mass. So those newly generated local swirls are made of positive ions, and these local swirl directions represent the electric current direction. Using the right hand rule, the clock-wise current (in Figure 5a, top view) will induce a bar magnet with S-pole towards to the reader (or N-pole away from the reader). As for electrons, they follow the background movement, so their effect can be cancelled out. So these west-spin positive ion swirls form many local (right hand) S-pole up (or N-pole down) magnetic bars.

Then (in Figure 6b, side view), in the θ-dimension of the 69%R to 75%R spherical shell, all these small S-pole up magnetic bars (see Figure 6b left side) are added together to form a single big S-pole up magnetic bar across the Sun (see Figure 6b right side). This explains Sun's magnetic field that is generated by the Tachocline zone high latitude region's convection. For easy explanation, let us suppose this part (the Tachocline zone high latitude region's convection) generated +4 Gauss of magnetic field. Let's define that the "+" Gauss for Sun as that in the side view, it has the magnetic S-pole up (as in Figure 6b).

With above explanation, readers can easily understand how the rest part of convective zone generates magnetic field for Sun. Figure 5b illustrates how the Tachocline zone (69%R to 75%R) low latitude region (between +/- 30°)'s convection generates -2 Gauss to Sun's magnetic field. According to Figure 3a (or 3b), Tachocline zone at low latitude region has slower angular speed ω at the inner edge and fast ω at the outer edge, so the differential speed induces the eastward (or anti-clock) local swirls in the Tachocline zone, therefore the negative Gauss. Figure 5c illustrates how the convective zone (75%R to

95%R) generates zero Gauss of Sun's magnetic field (because there is no ω difference in this zone according to Figure 3b). Figure 5d illustrates how the convective Y*lm* cycle zone (95%R to 100%R) phase-1 generates -3 Gauss of Sun's magnetic field, because |nLL> mode convection generates faster eastward positive ion stream near equator, and it produces the negative Gauss. Figure 5e illustrates how the convective Y*lm* cycle zone (95%R to 100%R) phase-2 generates -1 Gauss of Sun's magnetic field, because |n,L,m=0..L-1> mode convection generates faster eastward positive ion stream at high latitude region, and it produces a weaker negative Gauss.

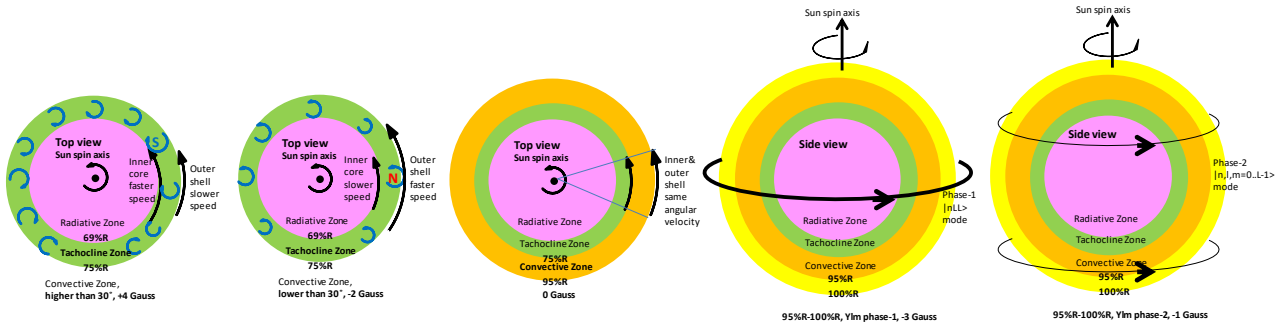

Figure 5 (from left to right: a, b, c, d, e). Green: Tachocline zone (69%R to 75%R), Orange: convective zone (75%R to 95%R), Yellow, Y*lm* cycle zone (95%R to 100%R). Notice that the thickness of each zone in figures 5a to 5e is not strictly based on the %R value.

Figure 5a. Illustration of how the Tachocline zone (69%R to 75%R) high latitude region's convection generates +4 Gauss of Sun's magnetic field.

Figure 5b. Illustration of how the Tachocline zone (69%R to 75%R) low latitude region's convection generates -2 Gauss of Sun's magnetic field.

Figure 5c. Illustration of how the convective zone (75%R to 95%R) generates zero Gauss of Sun's magnetic field.

Figure 5d. Illustration of how the convective Y*lm* cycle zone (95%R to 100%R) generates -3 Gauss of Sun's magnetic field in phase-1.

Figure 5e. Illustration of how the convective Y*lm* cycle zone (95%R to 100%R) generates -1 Gauss of Sun's magnetic field in phase-2.

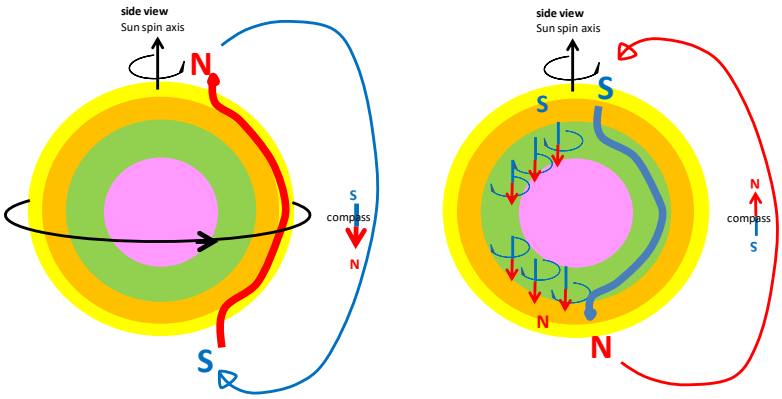

Figure 6a. The net effect of Sun's magnetic field in phase-1. It is dominated by the Y*lm* cycle zone (95%R to 100%R) phase-1 |nLL> mode convection generated strong magnetic field (condition-1). If this is correct, due to the current Sun has magnetic S-pole down, then the current Sun should be in phase-1 of the Y*lm* cycle.

Figure 6b. The net effect of Sun's magnetic field in phase-2. It is dominated by the Tachocline zone (69%R to 75%R) high latitude region's convection (condition-1).

Then, in phase-1, results from Figure 5a, 5b, 5c, 5d are added, (+4)+(-2)+(0)+(-3) = -1 Gauss, as shown in Figure 6a. In phase-2, results from Figure 5a, 5b, 5c, 5e are added, (+4)+(-2)+(0)+(-1) = +1 Gauss, as shown in Figure 6b. Please understand that the Gauss values are purely made up (by me) for easy explanation. So the better explanation is, the convective zone (from 69%R to 95%R) generates a constant N-pole down and a constant medium valued magnetic field. The Y*lm* cycle (95%R to 100%R) generates a constant N-pole up, but 11-years strong followed by 11 years weak magnetic field. So during one 11 years, Y*lm* cycle (95%R to 100%R)'s strong N-pole up overcome the medium valued 69%R~95%R N-pole down, and generates -1 Gauss N-pole up magnetic field for Sun (see Figure 6a). During the next 11 years, the medium valued 69%R~95%R N-pole down overcome the Y*lm* cycle (95%R to 100%R)'s weak N-pole up, and generates a +1 Gauss N-pole down magnetic field for Sun (see Figure 6b). This explains the oscillation of +/- 1 Gauss Sun magnetic field in Sun's 22 year period.

However, there is a weak point in this model. Here we only know that current Sun has its magnetic S-pole at south (see http://wso.stanford.edu/gifs/Polar.gif, and thanks WSO experts explained it to me). But I don't know among Figure 5d and Figure 5e, which one generates stronger magnetic field. So if (we make a big assumption that) Figure 5d has stronger magnetic field than that of Figure 5e (let us name it as "condition-1"), then the current Sun is in phase-1 of Y*lm* cycle (as shown in Figure 6a). On the other hand, if Figure 5d has weaker magnetic field than that of Figure 5e (let us name it as "condition-2"), then the current Sun is in phase-2 of Y*lm* cycle (as shown in Figure 7b. Then figures 6a and 6b are no longer correct).

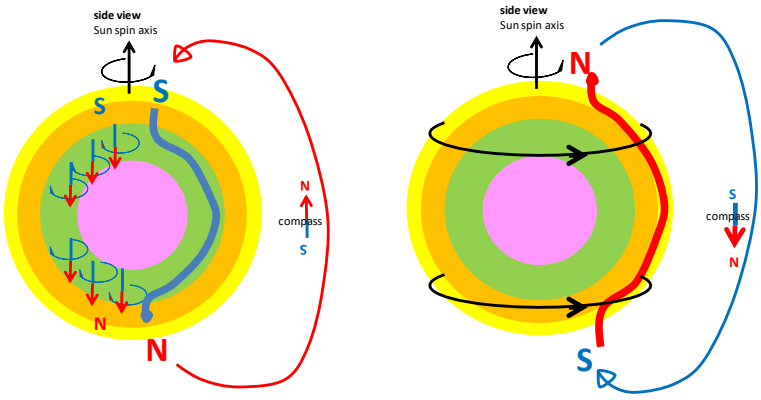

Figure 7a. The net effect of Sun's magnetic field in phase-1. It is dominated by the Tachocline zone (69%R to 75%R) high latitude region's convection (condition-2).
Figure 7b. The net effect of Sun's magnetic field in phase-2. It is dominated by the Y*lm* cycle zone (95%R to 100%R) phase-2 |n,L,m=0..L-1> mode convection generated strong magnetic field (condition-2). If this correct, since current Sun has magnetic S-pole down, then the current Sun should be in phase-2 of the Y*lm* cycle.

The explanation of Sun's magnetic dynamo is further complicated by the fact that the Sun's magnetic field reverses direction at the solar maximum. From wiki "sunspot", "*The point of highest sunspot activity during a cycle is known as solar maximum and the point of lowest activity as solar minimum*". From wiki "Stellar magnetic field", "*The Sun's major component of magnetic field reverses direction every 11 years (so the period is about 22 years), resulting in a diminished magnitude of magnetic field near reversal time. During this dormancy, the sunspots activity is at maximum* ".

To use Y*lm* cycle model to explain all of these phenomena, I constructed the Figure 8. The top line six Sun plots summarize the Y*lm* cycle model on Sun's surface. The green straight line represents the expected surface mass position (same φ value in the θφ-2D-dimension) if the Y*lm* cycle reset to zero. The pink line shows the real surface mass position during the Y*lm* cycle movement. Notice that the pink line overlaps with the green line at the beginning or end of the Y*lm* 22-years cycle. The first three Sun plots shows that the phase-1's |nLL> mode convection causes Sun surface mass at low

latitude moving ahead of those at high latitude. The last three Sun plots shows that the phase-2's |n,L,m=0..L-1> mode convection causes Sun surface mass at high latitude catching up to that of the low high latitude.

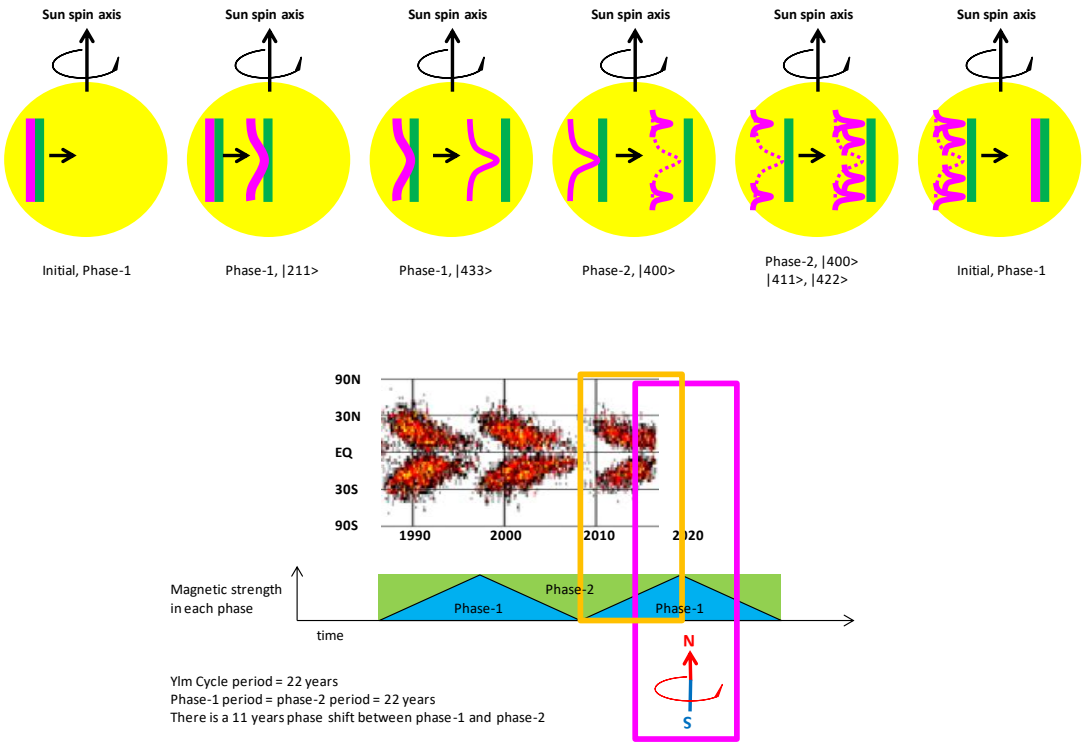

Figure 8. Using {N,n} QM and Y*lm* cycle model to explain Sun's magnetic dynamo and sunspot drift. Note: the phase-1 and phase-2 in the bottom plot is based on that the condition-1 is correct.

Now let me explain the middle and bottom line plots in detail. The middle line plot of Figure 8 shows the butterfly pattern of sunspot drift. The bottom line plot of Figure 8 shows how phase-1 and phase-2 alternates during the Y*lm* cycle (here suppose condition-1 (or Figure 6) is correct). Both plots have the same time x-axis as shown in the middle plot. Notice that the Y*lm* cycle period = 22 years, the period of either Phase-1 or phase-2 is also 22 years. This ends up both phase-1 and phase-2 have triangle shaped time curves, and with an 11 years of phase shift between them (see bottom plot). Now we need to make an assumption here: only the decreasing phase of Phase-1 (or Phase-2) produces sunspot. So the sunspots between year 1997 and 2008 were produced by the decreasing Phase-1 (in blue), and the sunspots between 2008 and 2019 are produced by the decreasing green Phase-2 (within the orange frame in both middle and bottom plots). So at 2018, we are currently at the end of Phase-2 caused sunspot period (if condition-1 is correct). For the orientation of the Sun's magnetic field, it is obviously determined by which one (among phase-1 and phase-2) is dominant. So from 2002 to 2013, it was Phase-2 (in green) dominant. From 2013 to 2024, it is Phase-1 (in blue) dominant (within the pink frame in both middle and bottom plots). Since we know current Sun has the magnetic S-pole downward (as shown below the bottom plot), therefore the phase-1 correlates to the Sun magnetic S-pole downward (if the condition-1 is correct). Then before 2013 it must be (the Sun magnetic S-pole) upward. So the Sun's magnetic field reverses at the middle of sunspot period (or at the solar maximum). Note: the scaling factor in Table 1 column 5 may have to change from 0.4x to 0.7x to adapt Figure 8 bottom plot.

Please notice that above results are based on the condition-1 (or Figure 6) is correct. If condition-2 (or Figure 7) is correct, then result is opposite. Readers can easily figure it out. I understand that with some unknowns (condition-1 vs. condition-2) and assumptions (sunspot only occurs at the 2nd half phase), this explanation is not a strong one. So further improvement of this explanation is needed.

From wiki "Tachocline", "*Recent radio observations of cooler stars and brown dwarfs, which do not have a radiative core and only have a convective zone, demonstrate that they maintain large-scale, solar-strength magnetic fields and display solar-like activity despite the absence of tachoclines. This suggests that the convective zone alone may be responsible for the function of the solar dynamo*". In 5 billion years, after all {-1,n=6..11}o orbit shells turns into convective zone, the Sun is expected to still have the magnetic field, because it still has the Tachocline zone (though it moves to ~ 25%R region) and Y*lm* cycle zone (still at 95%R to 100%R, details will be explained in a future SunQM paper). So for stars have no radiative zone, only convective zone, this model still generates star magnetic field.

III. Like sunspot drift, Earth's continental drift is also caused by the Y*lm* cycle which happens in Earth mantle {-1,3//4}o orbit shell

From wiki "Mantle (geology)", Earth's mantle "*is predominantly solid but in geological time it behaves as a viscous fluid*". From wiki "Supercontinent cycle", "*The supercontinent cycle is the quasi-periodic aggregation and dispersal of Earth's continental crust. …One complete supercontinent cycle is said to take 300 to 500 million years. Continental collision makes fewer and larger continents while rifting makes more and smaller continents*". Figure 9 shows how to use Y*lm* cycle model to explain Earth's continent drift and the supercontinent cycle.

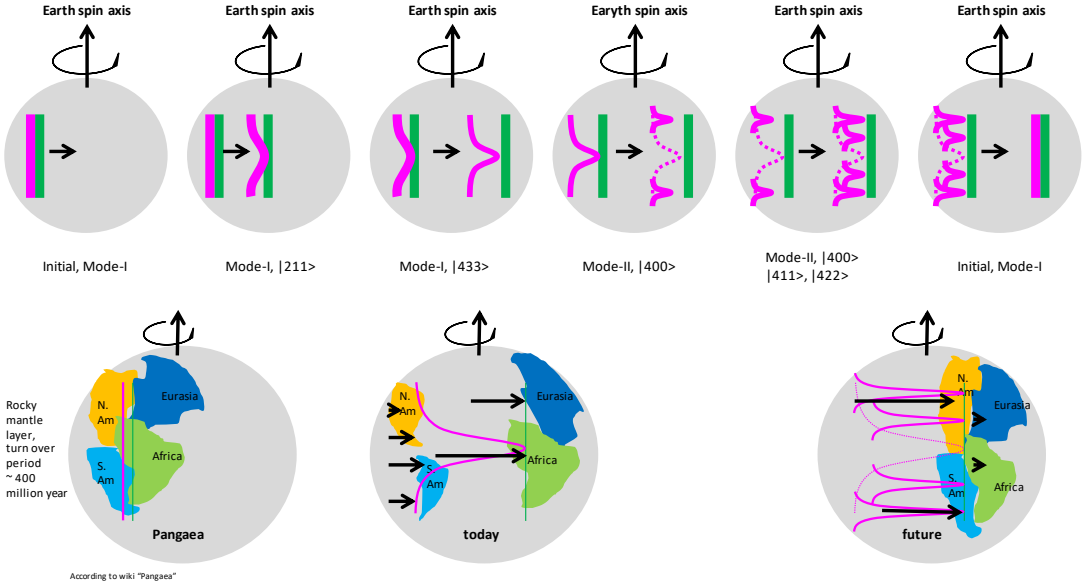

Figure 9. Using Y*lm* cycle model to explain Earth's continent drift and the supercontinent cycle.

From the analysis in paper SunQM-3s6, in a p{N,n//4} QM model, Earth's mantle belongs to the p{-1,3//4}o orbit shell. So it is much easier to use n=4 's Y*lm* cycle model to explain. As shown in the top line figures of Figure 9, the spinning of Earth causes the |211> (then to |433>, then to higher n of |nLL>) mode mass peaking in phase-1. Then it causes mass at the equator region to ooze out from the beneath of the mantle surface to the mantle surface (or from right below p{-1,4//4} to p{-1,4//4}), but still right beneath the crust. This oozed out mass carries the fast eastward movement, therefore forms the faster east moving zonal band at the equator region right below the Earth crust (or the tectonic plates).

Now let us start from a supercontinent, for example, Pangaea ~300 Mya (see Figure 9, bottom left figure "Pangaea"). Let us simplified the situation by consider only four major continents: North America, South America, Africa, and Eurasia. From the analysis results in section I, we know that in the Y*lm* cycle model, phase-1's |nLL> mode dominates the low latitude surface movement, and phase-2's |n,L,m=0..L-1> modes dominate the high latitude surface movement.

Because of its high latitude, North America continent's drift is dominated by the phase-2's |n,L,m=0..L-1> modes. Because of its relative high latitude at south hemisphere, South America continent's drift is mostly dominated by the phase-2's |n,L,m=0..L-1> modes. Because of its low latitude, Africa continent's drift is completely dominated by the phase-1's |nLL> mode. As for Eurasia continent, its eastward drifting is dominated by the push from the Africa continent. So in phase-1, Africa continent is carried by the fast moving equatorial zonal band underneath to the east with distance about 80/360 of Earth's circumference (see Figure 9, bottom middle figure "today"). Eurasia, pushed by the Africa continent, also moved eastward with distance about 80/360 of Earth's circumference. South America, although dominated by phase-2, but still partly affected by phase-1, also moved eastward with distance about 30/360 of Earth's circumference. Only North America is standing still (of cause, all other continents' movements are relative to North America). This analysis makes me to believe that currently we are at the middle or later stage of phase-1, because the Atlantic Ocean is still opening.

Then in phase-2, the mass peaking under |n,L,m=0..L-1> mode causes the high latitude mass to ooze out, and speed up high latitude region's eastward movement. Therefore, it carries both North America and South America moving to the east. Meanwhile, Africa continent will stop moving because the fast eastward moving equatorial zonal band has diminished. So to the end, the east moving North & South America continents will collide with the standing still Africa continent, form a new supercontinent, and finish one cycle of the supercontinent cycle (in about 150 My later, see Figure 9 bottom right figure 'future"). Of cause, Figure 9 bottom right figure over simplifies the future supercontinent formation, it does not include the self-rotation of each continent during drifting. This kind of Y*lm* cycle can be repeated many times. As the result, Y*lm* cycle QM model really supports the supercontinent cycle model.

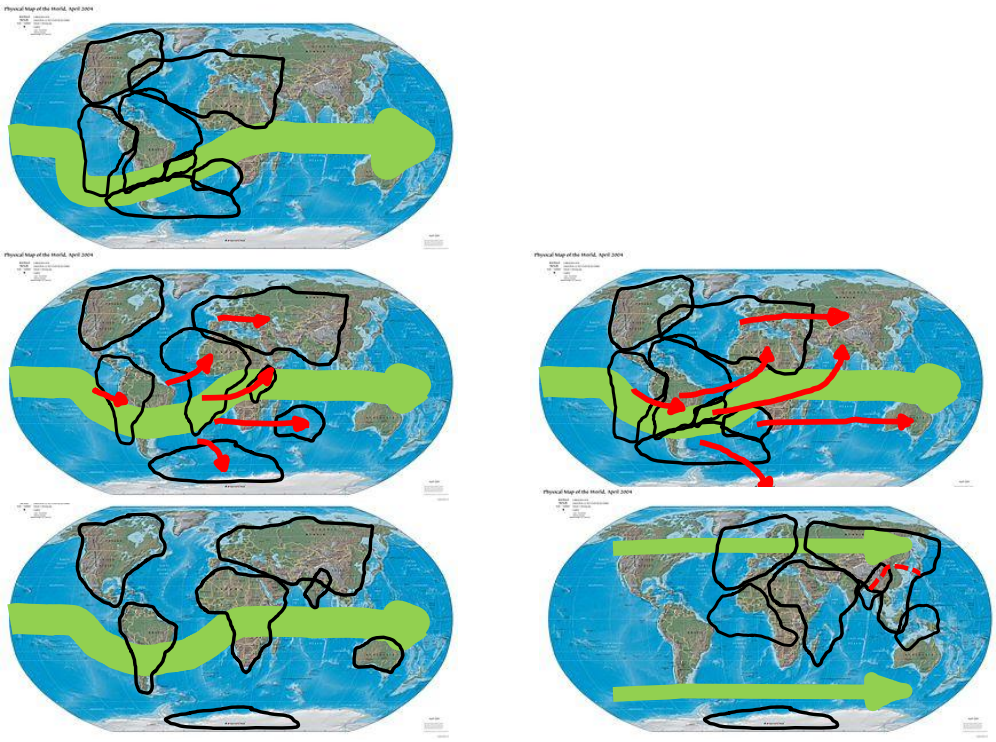

Figure 10. Using Y*lm* cycle model phase-1 to explain how Pangaea evolved into today's world map. Left top: Pangaea; Left middle: half way from Pangaea to today's map; Left bottom: today's map. Right middle: a summary of three left figures; Right bottom: hypothesized next supercontinent. The background world map is copied from wiki "List of mountain ranges", figure "*Physiographic world map with mountain ranges and highland areas* ...". Author: Physical World Map 2004-04-01 CIA World Factbook. Copy Right "Public Domain".

The driving force to onset the phase-1 of Y*lm* cycle for Earth's mantle shell is Earth QM's nLL disk-lyzation effect caused by Earth spin. The driving force to onset the phase-2 of Y*lm* cycle for Earth's mantle shell can be explained as: the extreme high viscosity of the rocky mantle forms the strong drugging force between each part, so at the end of phase-1, at 100%R, the moving ahead part at 0° latitude will drug the falling behind part at 30° latitude (in θφ-2D-dimension). And at the 30° latitude, the moving ahead ~95%R part will drug the falling behind 100%R part (in rφ-2D-dimension, due to the inner shell spin faster than the surface shell). So these two drugging forces will eventually onset the falling behind part (at 30° latitude and 100%R) to move to +φ direction, and start the |n,L,m=0..L-1> convection band. The explanation in section I-f is also applicable here.

A detailed explanation of all continents drift (including the Antarctica, India, Australia, besides the four mentioned in Figure 9) is given in Figure 10. The explanation is based on Y*lm* cycle phase-1 model's |nLL> mode, and also referenced figures "*The breakup of Pangaea over time*" and "*Animation of the rifting of Pangaea*" in wiki "Pangaea".

As explained before, Earth's p{N,n//4} QM structure caused Y*lm* cycle |433> mode mass peaking effect somewhere underneath the mantle surface. It produced a ring at equator, oozed out from the deep of mantle to the surface, carried faster eastward movement. However, this fast moving equatorial ring was blocked by a strong standing dam made of South America and North America continents. Then, according to hydrodynamics, the fast |nLL> flow stream would have to find a way to bypass the firmly standing South America (and North America). The easiest way was to go through the southern end of the South America, as shown in Figure 10 in green thick arrow. So instead of keeping on equator, this fast |nLL> flow stream was forced to go through underneath of the middle and southern part of South America continent. It forced South America continent to move eastward by 30/360 of Earth circumference, and rotated anti-clockwise by about 10 degree. Because of this, it also lifted the massive Andes Mountains at the west edge of South America continent at that time (see wiki "Andes", "*The formation of the modern Andes began with the events of the Triassic when Pangaea began the break up that resulted in developing several rifts*").

After bypassing the (South America continent) blocker, this fast |nLL> stream flowed back to equator. By doing so, it generated a big anti-clock rotational force besides the fast east moving force, and formed a gigantic anti-clock turbulent swirl (centered at Pangaea's Africa continent, including its eastside edge fragments India and Australia). Therefore, Africa continent was not only drifted to the east by 80/360 of Earth circumference, but also rotated by about 10 degree anti-clockwise. India continent, a small fragment at the edge of the gigantic Africa continent, was spun off from the edge of Africa continent by this rotation, and thrown to the northern hemisphere (by both east moving force and rotational force), and eventually crushed with the Eurasia continent (see Figure 10 left middle and left bottom). It must also have rotated more than 20 degree anti-clockwise. Australia continent was also spun off from the edge of Africa continent. Because it sat near the center of the fast |nLL> flow stream, and also because of its relative small size, it had been carried to as far as 130/360 of Earth circumference eastward. Because it sat at a little bit south of the fast |nLL> flow stream, it may have rotated 1 or 2 degrees clockwise.

Meanwhile, that the |nLL> mode caused mass oozed out to mantle surface at equator would have caused (a general) mantle surface mass flow from equator to the two poles sides. This formed the part of the force that driving India continent moving to the northern hemisphere (because it sat at the north side of the |nLL> fast flow stream). Antarctic continent, because sitting at the south side of the |nLL> fast flow stream, was pushed to further south by this force. It may also be rotated a few degrees clockwise because of this movement. In this way, we can see that the apparent random drifting of post-Pangaea continents can be nicely depicted as an expected hydrodynamic result of a broken dam through a mouth located near the south end of South America continent (see Figure 10 left-top and left middle). The key reason why this was happening is that the Y*lm* phase-1 |nLL> mode produced a strong eastward flow stream and it was blocked by a dam (South America and North America).

Both North American plate and South American plate have a sharp coastline head at west, and a long tail (of seabed) at east, especially the south end of South American plate has a very long tail to the east. To me it is strong evidence that these two plates are standing there to against a strong force coming from the west.

The most recent continental drift (during last 150 million years, driven by Y*lm* cycle phase-1) generated two Earth-scale mountain systems: the Alpine-Himalayan system, caused by the collision of both Africa and India continents to the Eurasia continent, and the Cordilleran-Andean system, caused by the collision of the Pacific plate to the North and the South American plates. The best map is shown in book "Earth portrait of a planet" (by Stephen Marshak, 4th ed. pp 456, figure

13.23). This map shows that the width of the mountain system (or the depth crossing the mountain system) is ~ 1000 km for Alpine-Himalayan system, ~ 1000 km for the North America Cordilleran system, and ≤ 500 km for the Andean system. We can easily imagine that how strong the Eurasia plate standing still to against the collision of Africa and India plates to generate 1000 km depth (in θφ-dimension, not in r-dimension) of mountain system (especially at Tibet). Similarly, the 1000 km depth (also in θφ-dimension, not in r-dimension) of North America Cordilleran system shows how strong the North American plate standing still to against the collision of Pacific plate, and the ≤ 500 km depth of Andean system shows that the South American plate is also strong, but less strong than that of the North American plate. So it justifies that while the South America continent has been drifting eastward by 30/360 of Earth circumference, the North America continent is (relatively) standing still.

Scotia Arc, an island arc system between the south tip of the South America continent and the Antarctic continent, has its arc points to the east. Under current leading tectonic plate theory, "*The formation of the Scotia Arc was initiated by an acceleration in South America's westward migration in the mid-Cretaceous (120 to 83 million years ago, Ma)*" (from wiki "Scotia Arc", and see figure "*Bathymetry of the Scotia Arc*"). However, in my view, this is the direct evidence that it is a mouth of a broken dam caused by the eastward convective mantle flow stream driven by the Y*lm* cycle phase-1 |nLL> mode. So if my model is correct, then we need to make some modification on the current tectonic plate theory: the South America is not migrating westward, it is migrating slowly eastward (relative to the standing still North America), partly because the continent is moving slowly to the east, also partly because the continent is self-rotating anti-clockwise. Crossing the Scotia Arc, the shore of the Antarctic continent is likely migrating eastward also due to that the continent itself is slowly rotating clockwise.

Besides that, I'd like to make a suggestion to the "Tectonic plates boundaries world map with their movement vectors and selected hotspots": https://upload.wikimedia.org/wikipedia/commons/a/aa/Tectonic_plates_boundaries_physical_World_map_Wt_180degE_centered-en.svg. If the author reset North America's movement vector to zero, and change the rest vectors coordinately, it would be more intuitive to see how the current tectonic plates are moving.

From wiki "Pangaea", Pangaea "*assembled from earlier continental units approximately 335 million years ago, and it began to break apart about 175 million years ago*". Now we are most likely at the later stage of phase-1, which means the early part of phase-2 in Y*lm* cycle may begin to start. At the end of phase-1, North America is the only continent that still stays at its (relative) original position. According to Y*lm* cycle theory, the major indication of the onset of phase-2 would be the North America plate start to move eastward. Therefore, I believe that the forming of Rocky Mountains (at high latitude +40˚ to +60˚) between ~80 Mya and 35Mya may indicate an early (and noisy) onset of phase-2 (see wiki "Rocky Mountains", "*The Rocky Mountains formed 80 million to 55 million years ago during the Laramide orogeny, in which a number of plates began sliding underneath the North American plate*"). The other evidence may include that "*Laramide orogeny period of mountain building in western North America, … started in the Late Cretaceous, 70 to 80 million years ago, and ended 35 to 55 million years ago. ... from Canada to northern Mexico, with the easternmost extent of the mountain-building represented by the Black Hills of South Dakota"* (see wiki "Laramide orogeny"). Re-activation of the Yellow Stone super volcano may also be part of the (noisy) onset of phase-2. In this way, Earth's continental drift is explained by the Y*lm* cycle which is happening right now in Earth mantle {-1,3//4}o orbit shell.

By combining Y*lm* cycle model with the general hydrodynamics knowledge, plus the geologic fossil record, the paleomagnetism knowledge and other knowledge, scientists will not only be able to map out the previous and future supercontinents more accurately, but also be able to construct the dynamic process of the supercontinent cycle. In this way, not only astronomy, but also geology can be studied by using QM.

Based purely on the Y*lm* cycle and the general hydrodynamic knowledge, I have guessed the next supercontinent (about 150 millions years later?) as shown in Figure 10 right bottom figure. Driven by the Y*lm* cycle phase-2's high latitude eastward moving mantle, both North America and South America continents will move to east and collide with the standing still Africa continent. The South America continent will have rotated about 60 more degrees anti-clockwise before the collision. The major part of Eurasia continent (including the west and north Eurasia) will move eastward significantly relative to (the relatively standing still) Africa continent. However, the southern Asia and eastern Asia will mostly standing still. The Australia continent will move northward, and collide with the south Asia near the equator, uplift and generate more land for south Asia. Furthermore, the intruding of India continent into the Eurasia continent may have a good chance to break the

east-south Asia from the major (west-north) Eurasia continent (see the red dashed line in Figure 10 right bottom plot). So the east region of the next supercontinent may be composed of (from north-west to south-east): the major (west-north) part of Eurasia continent, the India continent, the new (east-south) Asia continent, and the Australia continent. It is hard to predict the future position for Antarctic continent from Y*lm* cycle model due to it sits at the pole.

IV. Using {N,n} QM and Y*lm* cycle model to explain Earth's magnetic dynamo

Earth's magnetic dynamo can also be explained by using Y*lm* cycle model. As shown in Figure 11, Earth inner (solid iron) core has a relative faster eastward spin, and mantle has a relative slower eastward spin. Again, for the macro-scaled Earth spin, the positively charged Fe ion and negative free electron produced magnetic fields are cancelled out. The differential spin speed produces many westward convective local turbulent swirls (shown in blue in Figure 11) inside the outer core (or the liquid iron core, shown in green shell in Figure 11). Again, this convection only affects the large mass particles like Fe ion, and has almost no effect on low mass particles like electron. So the local swirls of Fe ions produce westward circular electric current, which in turn generates many small magnetic S-pole up bar magnets (see Figure 11 left side). The combination of all these local bar magnets forms a total bar magnet through Earth outer core with the magnetic S-pole up (see Figure 11 right side). Since current Earth's magnetic field is magnetic S-pole up, so right now our Earth's magnetic dynamo is dominated by the westward local circular electric current inside Earth outer core (as shown in Figure 11). Figure 11 is evolved from the Dynamo theory (see wiki "Dynamo theory" figure "*Illustration of the dynamo mechanism that creates the Earth's magnetic field*").

Besides local swirls, Y*lm* cycle at the outer edge of the liquid iron core also makes critic contribution to the orientation of Earth's magnetic field. As shown in Figures 5d and 5e, the magnetic field produced by Y*lm* cycle is always opposite to that produced by the local swirls. So a strong Y*lm* magnetic field will overcome the local swirls' magnetic field, and reverse the direction of current Earth's magnetic field. Again, since we don't know which phase (among phase-1 and phase-2) produces the stronger magnetic field, we are not able to know current Earth magnetic field belongs to phase-1 or phase-2 of Y*lm* cycle.

Please notice that Earth's magnetic field is produced in Earth's outer core, or in Earth QM structure's p{-1,2//4}o orbit space. According to wiki "Earth's magnetic field", Earth magnetic field "*Reversals occur nearly randomly in time, with intervals between reversals ranging from less than 0.1 million years to as much as 50 million years. The most recent geomagnetic reversal ... occurred about 780,000 years ago*". So it has period (which equals to a full Y*lm* cycle period) greater than 1E+5 years. In comparison, Earth's continent drift results from the Y*lm* cycle in Earth's mantle, or in Earth QM structure's p{-1,3//4}o orbit space. It has period (which equals to a full Y*lm* cycle period) around 300 ~ 500 million years.

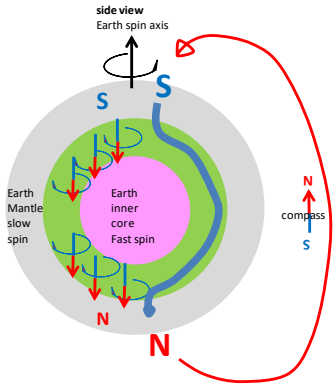

Figure 11. Since current Earth's magnet field is magnetic S-pole up, its magnetic dynamo is dominated by the westward local circular electric current (as shown in blue swirls) inside liquid iron shell (as shown in green shell).

V. Y*lm* cycle effect on other planets' atmosphere and magnetic field

The Y*lm* cycle effect must also exist in Jupiter (and Saturn, Neptune, Uranus, and even Earth) atmosphere's cloud pattern, although it may be pretty weak and noisy so that it is less obvious. Jupiter's |544> zonal band sometimes is divided into two sub-bands (by a middle thin belt). As seen in SunQM-3s3 Figure 5 (copied from wiki "Atmosphere of Jupiter" figure "*zonal wind speeds in the atmosphere of Jupiter*"), the zonal wind speed at 0 degree latitude is slower than that at +/- 8 degree latitude. Its |5,4,m=0..3> zonal bands may also have similar phenomenon momentarily. It happens to Saturn too (see paper SunQM-3s3 Figure 6c, copied from wiki "Planetary core"). I believe that these phenomena can also be explained by the Y*lm* cycle model, although it needs to add more complicated modes. Let us name the |n,L,m=0..L> zonal bands (on atmospheric surface of Jupiter, Saturn, etc.) described in paper SunQM-3s3 as the "primary zonal band", and name the Y*lm* cycle induced zonal bands as the "secondary zonal band". From the phenomena mentioned above, I guess that for gas/ice planets' atmosphere, the secondary (and gradually narrowing) zonal band happens on top of all the primary zonal bands. The phase-1 (narrowing) secondary zonal bands are less obvious because their backgrounds are the strong primary zonal bands. However, the phase-2 (narrowing) secondary (effective belt) bands are more obvious because their produce effective high n |n,L,m=0..L-1> belt bands at the middle of the primary zonal bands (with low n of |nLL>), so that the primary zonal bands looks like two sub-bands. We need more accurate observation data before we can determine the more accurate Y*lm* model for the explanation.

Similarly, Y*lm* cycle is expected to cause the planetary magnetic field reversal for all planets. Table 3 shows a table summary of Y*lm* cycle for Sun and planets:

Table 3. A table summary of Y*lm* cycle for Sun and planets

Ylm cycle	phenomenon	produced in	{N,n} QM structure	function of phase-1	function of phase-2	function of Y*lm*	period, year
Sun	sunspot drift	95%R to 100%R	{-1,11}o	butterfly pattern	butterfly pattern	---	22
Sun	magnetic field reversal	95%R to 100%R	{-1,11}o	---	---	reverse magnetic field	22
Earth	continent drift	mantle surface	p{-1,3//4}o	continent rift	continent collide	---	3E+8 ~ 5E+8
Earth	magnetic field reversal	liquid iron core surface	p{-1,2//4}o	---	---	reverse magnetic field	from 1E+4 to 5E+7
Jupiter	?						
Saturn	?						
Uranus	?						
Neptune	?						

Conclusion

Y*lm* cycle model with two phases has been proposed. In phase-1 of Y*lm* cycle, the |nLL> QM mode's mass peaking and upwelling effect generates a fast flow ring near the equator at the surface of a {N,n} QM orbit shell. As phase-1 evolves, the n quantum number become higher, the fast flow ring become narrower, shallower and faster, and then diminishes in the end (because it will be too narrow, too shallow to sustain). In phase-2 of Y*lm* cycle, the |n,L,m=0..L-1> QM mode's mass peaking and upwelling effect generates an effective slow flow ring near the equator at the surface of a {N,n} QM orbit shell. As phase-2 evolves, the n number become higher, the effective slow flow ring become narrower, shallower, and then diminishes in the end. In current paper, Y*lm* cycle model has been successfully used to explain the butterfly pattern of sunspot drift. Sunspots are the turbulent swirls at the interface between the fast flow and slow flow bands. The same Y*lm* cycle has also been used to explain Earth's continental drift and the supercontinent cycle. Furthermore, the same Y*lm* cycle model can be used to explain both Sun's and Earth's magnetic dynamo. The alternation between phase-1 and phase-2 controls the reversal of Sun's or Earth's magnetic field.

References

[1] Yi Cao, SunQM-1: Quantum mechanics of the Solar system in a {N,n//6} QM structure. http://vixra.org/pdf/1805.0102v2.pdf （original submitted on 2018-05-03）

[2] Yi Cao, SunQM-1s1: The dynamics of the quantum collapse (and quantum expansion) of Solar QM {N,n} structure. http://vixra.org/pdf/1805.0117v1.pdf （submitted on 2018-05-04）

[3] Yi Cao, SunQM-1s2: Comparing to other star-planet systems, our Solar system has a nearly perfect {N,n//6} QM structure. http://vixra.org/pdf/1805.0118v1.pdf （submitted on 2018-05-04）

[4] Yi Cao, SunQM-1s3: Applying {N,n} QM structure analysis to planets using exterior and interior {N,n} QM. http://vixra.org/pdf/1805.0123v1.pdf （submitted on 2018-05-06）

[5] Yi Cao, SunQM-2: Expanding QM from micro-world to macro-world: general Planck constant, H-C unit, H-quasi-constant, and the meaning of QM. http://vixra.org/pdf/1805.0141v1.pdf （submitted on 2018-05-07）

[6] Yi Cao, SunQM-3: Solving Schrodinger equation for Solar quantum mechanics {N,n} structure. http://vixra.org/pdf/1805.0160v1.pdf （submitted on 2018-05-06）

[7] Yi Cao, SunQM-3s1: Using 1st order spin-perturbation to solve Schrodinger equation for nLL effect and pre-Sun ball's disk-lyzation. http://vixra.org/pdf/1805.0078v1.pdf （submitted on 2018-05-02）

[8] Yi Cao, SunQM-3s2: Using {N,n} QM model to calculate out the snapshot pictures of a gradually disk-lyzing pre-Sun ball. http://vixra.org/pdf/1804.0491v1.pdf （submitted on 2018-04-30）

[9] Yi Cao, SunQM-3s3: Using QM calculation to explain the atmosphere band pattern on Jupiter (and Earth, Saturn, Sun)'s surface. http://vixra.org/pdf/1805.0040v1.pdf （submitted on 2018-05-01）

[10] SunQM-3s6: Predict mass density r-distribution for Earth and other rocky planets based on {N,n} QM probability distribution. http://vixra.org/pdf/1808.0639v1.pdf (submitted on 2018-08-29)

[11] SunQM-3s7: Predict mass density r-distribution for gas/ice planets based on {N,n} QM probability distribution. http://vixra.org/pdf/1812.0302v1.pdf (submitted on 2018-12-17)

[12] SunQM-3s8: Using {N,n} QM to study Sun's internal structure, convective zone formation, planetary differentiation and temperature r-distribution. http://vixra.org/pdf/1808.0637v1.pdf (submitted on 2018-08-29)

[13] Neil F. Comins & William J. Kaufmann, "Discovering the Universe", pp328, Figure 10-13, Babcock's magnetic dynamo.

[14] Christensen-Dalsgaard J. & Thompson, M.J. (2007). The Solar Tachocline: Observational results and issues concerning the tachocline. Cambridge University Press. pp. 53–86.

[15] A series of my papers that to be published (together with current paper):
SunQM-3s9: Using {N,n} QM to explain the sunspot drift, the continental drift, and Sun's and Earth's magnetic dynamo.
SunQM-3s10: Updates and Q/A for SunQM series papers.
SunQM-3s4: Using {N,n} QM structure and multiplier n' to analyze Saturn's ring structure.
SunQM-3s5: Using {N,n} QM structure and n*l*0 effect to analyze the Bipolar outflow.
SunQM-5: A new version of QM based on interior {N,n}, multiplier n', |R(n,l)|^2 |Y(l,m)|^2 guided mass occupancy, and RF, and its application from string to universe.
SunQM-5s1: White dwarf, neutron star, and black hole re-analyzed by using the internal {N,n} QM.

[16] Major QM books, data sources, software I used for this study are:
Douglas C. Giancoli, Physics for Scientists & Engineers with Modern Physics, 4th ed. 2009.
John S. Townsed, A Modern Approach to Quantum Mechanics, 2nd ed., 2012.
David J. Griffiths, Introduction to Quantum Mechanics, 2nd ed., 2015.
Stephen T. Thornton & Andrew Rex, Modern Physics for scientists and engineers, 3rd ed. 2006.
James Binney & David Skinner, The Physics of Quantum Mechanics, 1st ed. 2014.
Wikipedia at: https://en.wikipedia.org/wiki/
Online free software: WolframAlpha (https://www.wolframalpha.com/)
Online free software: MathStudio (http://mathstud.io/)
Free software: R
Microsoft Excel.
Public TV's space science related programs: PBS-NOVA, BBC-documentary, National Geographic-documentary, etc.
Journal: Scientific American.